Correlation effects for electron-positron momentum density in solids

B. Barbiellini,* M. Hakala,† M. J. Puska,‡ and R. M. Nieminen§
Laboratory of Physics, Helsinki University of Technology, FIN-02150 Espoo, Finland

A. A. Manuel‖
Department of Physics, University of Geneva, 24 Quai E. Ansermet, 1211 Geneva 4, Switzerland
(Received 23 December 1996; revised manuscript received 22 May 1997)

A method describing the calculation of the momentum density of annihilating electron-positron pairs in solids has been developed. One-electron states, which are not perturbed by the positron, are used. The effects due to the enhancement of the electron density near the positron are taken into account by a factor depending on the electron state in the annihilating pair. This enhancement is used both for the valence and core electron states. The calculated momentum densities are in good agreement with the two-dimensional angular correlation of the annihilation radiation measurements in defect-free Cu and GaAs. [S0163-1829(97)02336-9]

I. INTRODUCTION

The measurement of the momentum distribution of annihilating electron-positron pairs is, together with the positron lifetime measurements, the basic method of positron annihilation spectroscopy.[1,2] The first measurements of the momentum distributions were performed with the angular correlation apparatus using a long-slit geometry. This gives the momentum distribution integrated over two perpendicular directions. The two-dimensional systems enable the measurement of momentum distributions integrated only in one direction. Three-dimensional momentum distributions have also been reconstructed from the results of two-dimensional measurements.[3] The measurement of the line shape of the Doppler-shifted annihilation spectrum also gives a momentum distribution integrated over two dimensions. Along with the experimental activity, electronic-band-structure calculation methods have been used to predict the momentum distributions.[4] One of the key questions in these calculations has been how to incorporate the electron-positron interactions into the theory.[5]

In this work we study the effects of the electron-positron interactions in the momentum distributions of annihilating electron-positron pairs. We present a general scheme that can be used in practical calculations devoted to quantitative comparisons between theoretical and experimental momentum distributions. We use a model developed previously to describe the momentum distributions corresponding to the core electrons.[6] In the model the effects due to the enhancement of the electron density at the positron are taken into account by a factor depending on the electron state in the annihilating pair. Now we generalize the model also to the valence electrons and obtain the total momentum distributions. The valence electron states having wave functions with a richness of different features serve as an optimal testing ground for the theoretical approach. Moreover, the results can be compared with high-resolution two-dimensional angular correlation of the annihilation radiation (2D-ACAR) spectra, which give detailed information also through the anisotropies of the momentum distribution.

The organization of the present paper is as follows. In Sec. II we review the most important aspects of the calculation of the electron-positron momentum distributions and describe the model used in this work. Section III is devoted to the results: First we compare the theoretical and experimental results for positrons in Cu, mainly in order to test the ability of the theory to describe the amplitude variations as a function of the magnitude of the momentum. Then, in the case of GaAs, we study more carefully the anisotropy of the distribution. In Sec. IV we present the conclusions.

II. THEORY

A. Momentum distribution of annihilating electron-positron pairs

The momentum distribution of annihilating electron-positron pairs can be written as

$$\rho(\mathbf{p}) = \pi r_e^2 c \sum_i \left| \int d\mathbf{r}\, \exp(-i\mathbf{p}\cdot\mathbf{r})\, \psi_i^{ep}(\mathbf{r},\mathbf{r}) \right|^2, \qquad (1)$$

where $\mathbf{p}$ is the total momentum of the annihilating pair, r_e the classical electron radius, and c the speed of light. The summation is over all occupied electron states. $\psi_i^{ep}(\mathbf{r},\mathbf{r})$ is the two-particle wave function when the positron and electron reside in the same point. $\psi_i^{ep}(\mathbf{r},\mathbf{r})$ can be further written by the help of positron and electron single-particle wave functions $\psi_+(\mathbf{r})$ and $\psi_i(\mathbf{r})$, respectively, and by the so-called enhancement factor $\gamma_i(\mathbf{r})$ as[7]

$$\psi_i^{ep}(\mathbf{r},\mathbf{r}) = \psi_+(\mathbf{r})\,\psi_i(\mathbf{r})\sqrt{\gamma_i(\mathbf{r})}. \qquad (2)$$

The enhancement factor takes into account the electron-positron interactions. If it equals unity one obtains the independent particle model (IPM).

The enhancement factor is a manifestation of the electron-positron correlations. The enhancement of the electron density at the positron is a crucial ingredient when calculating the *total* positron annihilation rate, which is the integral of $\rho(\mathbf{p})$ over the momentum $\mathbf{p}$. The *shape* of the momentum distribution of the annihilating electron-positron pairs is reasonably well described without the electron-positron interac-

tions, i.e., within the IPM (Ref. 1) if only the sp valence electron contribution is considered. However, when one constructs the total momentum distribution, for example, for Cu, the IPM fails to give the correct relative weights for the sp and d valence electron contributions.[8]

Many-body calculations for a delocalized positron in a homogeneous electron gas have been used to model the electron-positron correlation.[9–11] When a positron is immersed in an electron gas the Coulomb attraction produces a cusp in the electron density at the positron site.[9–11] The cusp determines the enhancement factor and contributes to the positron-electron correlation energy. The results for the homogeneous electron gas can be successfully applied in calculating positron annihilation rates for real solids with inhomogeneous electron densities.[12] Calculations for a positron in a homogeneous electron gas have also been used to estimate the correlation effects in the momentum distributions. Kahana[13] employed a Bethe-Goldstone-type ladder-diagram summation and predicted that the annihilation rate increases when the electron momentum approaches the Fermi momentum p_F in metals. This momentum dependence is explained by the fact that the electrons deep inside the Fermi liquid cannot respond as effectively to the positron as those near the Fermi surface. According to the many-body calculations by Daniel and Vosko[14] for the homogeneous electron gas the electron momentum distribution is lowered just below the Fermi level. This Daniel-Vosko effect would oppose the increase of the annihilation rate and the peaking of the electron-positron momentum distribution. In any case, one can define a momentum-dependent enhancement factor

$$\gamma(p)=\rho(p)/\rho^{\mathrm{IPM}}(p), \tag{3}$$

where $\rho^{\mathrm{IPM}}(p)$ is the IPM partial annihilation rate. Stachowiak[11] has proposed a phenomenological formula for the momentum dependence in electron gas as

$$\frac{\gamma(p_F)-\gamma(0)}{\gamma(0)}\simeq 0.13 r_s, \tag{4}$$

where $r_s=(3/4\pi n)^{1/3}$ and n is the electron density. According to Stachowiak the result is quite sensitive to the construction of the many-body wave function. Experimentally, the peaking of the momentum density at p_F should, in principle, be observable in alkali metals. However, different experiments disagree[8] and, moreover, it may be very difficult unambiguously to extract the valence from the core contribution because of the presence of oxide layers on alkali metal samples.[15]

The Bethe-Goldstone equation in the plane-wave representation (corresponding to the homogeneous electron gas) can be generalized by using Bloch wave functions for a periodic ion lattice. This approach has been reviewed by Sormann.[16] The conclusion is that the state dependence of the enhancement factor is strongly modified by the inhomogeneity and the lattice effects. Therefore, in materials that are not nearly-free-electron-like, the Kahana momentum dependence of $\gamma(\mathbf{p})$ is probably completely hidden. However, plane-wave-type expansions are poorly convergent to handle the electron-positron correlation cusp. Choosing more appropriate functions depending on the electron-positron relative distance r_{12} may provide more effective tools to deal with the problem.

A widely used method to incorporate many-body effects into the calculation of the momentum density is based on the local-density approximation (LDA).[5,7,17] The simplest LDA enhancement factor in Eq. (1) depends only on the local electron density at the positron site,

$$\gamma_i(\mathbf{r})=\gamma_{\mathrm{LDA}}(n(\mathbf{r})) \tag{5}$$

and its effect is similar to that of including the positron wave function[17] in the calculation of the momentum distribution. This enhancement has been used for metals,[17] semiconductors,[18–20] and also for high-T_c oxides.[21] The LDA enhancement factor for metals introduced by Daniuk *et al.*[7] has also a Kahana-type energy dependence. The LDA enhancement factor can also be improved by including the dependence on the gradient of the electron density,[12] i.e.,

$$\gamma_i(\mathbf{r})=\gamma_{\mathrm{GGA}}(n(\mathbf{r}),|\nabla n(\mathbf{r})|). \tag{6}$$

The ensuing method is called the generalized-gradient approximation (GGA) for the positron annihilation rate. The LDA and its GGA generalization for calculating the momentum density usually improve the agreement with experiments with respect to the IPM results. The GGA gives slightly better results than the LDA.[12] However, both the GGA and the LDA result in spurious oscillations with respect to the experimental data.[5,6]

B. The present method

The purpose of this work is to present a general scheme for calculating $\gamma_i(\mathbf{r})$ such that it can be used in practical calculations devoted to quantitative comparisons between theoretical and experimental momentum distributions. First, we note that under the requirements given in Ref. 9 the Bethe-Goldstone equation is equivalent to the Schrödinger equation for the pair wave-function $F(\mathbf{r}_1,\mathbf{r}_2)$ describing an electron and a positron interacting via a screened Coulomb potential.[9] The Pluvinage approximation[22] for $F(\mathbf{r}_1,\mathbf{r}_2)$ consists in finding two functions $G(\mathbf{r}_1,\mathbf{r}_2)$ and $f(\mathbf{r}_1,\mathbf{r}_2)$ such that $F(\mathbf{r}_1,\mathbf{r}_2)=G(\mathbf{r}_1,\mathbf{r}_2)f(\mathbf{r}_1,\mathbf{r}_2)$ and such that the Schrödinger equation becomes separable. $G(\mathbf{r}_1,\mathbf{r}_2)$ describes the orbital motion of the two particles ignoring each other, and $f(\mathbf{r}_1,\mathbf{r}_2)$ describes the correlated motion. The correlated motion depends strongly on the initial electron state i (without the presence of the positron). Obviously, the localized electron states near the nuclei are less affected by the positron than the sp-type valence orbitals.

We have developed, on the basis of the Pluvinage approximation, a theory for the momentum density of annihilating electron-positron pairs.[6] In practice, it leads to a scheme in which we first determine the momentum density for a given electron state i within the IPM. When calculating the total momentum density this contribution is weighted by

$$\gamma_i=\lambda_i/\lambda_i^{\mathrm{IPM}}, \tag{7}$$

where λ_i is the partial annihilation rate of the electron state i (including correlation effects) and λ_i^{IPM} is the same quantity

in the IPM. This means that a state-dependent enhancement factor γ_i substitutes $\gamma_i(\mathbf{r})$ in Eq. (1). The partial annihilation rate λ_i is obtained as

$$\lambda_i = \pi r_e^2 c \int d\mathbf{r} n_i(\mathbf{r}) \gamma_{\mathrm{LDA,GGA}}(\mathbf{r}), \tag{8}$$

where $n_i(\mathbf{r})$ is the electron density for the state i. If this theory is applied to the homogeneous electron gas it leads to the same constant enhancement factor to all electron states, i.e., there is no Kahana-type momentum dependence [Eq. (3)] in the theory. In practice, we calculate $\gamma(\mathbf{r})$ using the GGA for the positron annihilation rate.[12] The GGA predicts for various solid systems positron lifetimes (inverses of the total annihilation rates) in good agreement with the experimental results.[12] Compared to the LDA, the GGA suppresses the electron-positron correlations and reduces especially the partial annihilation rates for the core states.

The theory described gives momentum distributions for the localized core electron states in good agreement with those measured by Doppler broadening techniques.[6,23] This is true for positrons delocalized in perfect crystal lattices as well as for positrons localized at vacancies in solids. In the previous calculations electron wave functions of free atoms have been used.[6,23] This is a reasonable approach for localized core states in solids but not for valence-band states. For valence electron states we now calculate the true band structures and use the corresponding wave functions when calculating the momentum distributions. This means that partial annihilation rates and momentum distributions for different **k**-point states in the first Brillouin zone and for different bands have to be determined. The ensuing first-principles state-dependent treatment of the enhancement effects justifies some phenomenological approaches,[24–26] in which the correlation factor depends on the electron binding energy.

The partial annihilation rates for different core electron states are relatively small. Their prediction forms already a stringent test bench for the theory describing the overlap of the electron and positron wave functions and the annihilation rate. The previous comparisons[6] with the results of Doppler broadening measurements show that the theory agrees reasonably well both for delocalized and localized positron states. For the core states a simplifying fact is that, in a given system, the core annihilation takes place only with a few core electron states and the atomic wave functions can be used for them. On the other hand, the valence electron states with widely different spatial distributions and with large partial annihilation rates serve an ideal testing ground for a quantitative theory.

The present calculations are much heavier than the previous ones,[6] which are well suited for a fast analysis of high-momentum ($\sim > 15\times 10^{-3} m_0 c$, m_0 is the electron mass) experimental data arising from Doppler measurements. Compared to the previous work, the present type of calculations will improve remarkably this analysis by avoiding the difficulty that one should be able to distinguish between core and valence states. Moreover, the valence electrons may also contribute at these high momenta. This is now properly taken into account.

III. RESULTS AND DISCUSSION

A. Shape of the momentum distribution

In order to test the present scheme of the state-dependent enhancement factor in the case of valence electrons we have made calculations for the momentum density of annihilating electron-positron pairs in the perfect Cu lattice. For the bulk Cu the IPM calculations give distributions that deviate remarkably from those measured by the 2D-ACAR.[27,28] The deviation indicates that for the d electrons the enhancement is smaller than for the sp conduction electrons. In more detail, it has been noted that for the $3d$ electrons in Ni and Cu, a constant enhancement factor is not adequate, but an enhancement factor depending on the electron state within the d band gives already a fairly good description.[24,25] Jarlborg and Singh[17] gave for this notion the following explanation. For a filled band the antibonding states near the top of the band are more localized around the nuclei than the bonding states near the bottom of the band. For states residing more in the interstitial region (with a lower electron density) the electron-positron correlation effects are stronger than for states localized closer to the nuclei. This model is in good agreement with the experimental analyses of Refs. 24 and 25. Below we illustrate that the interplay between the bonding and antibonding states and the enhancement factor is valid also in our present model, although the hybridization of bands makes the dependencies diffuse.

To perform a complete study we have considered the actual Bloch states in Cu with a mixed sp and d character. First, the self-consistent electronic structure is obtained with the linear-muffin-tin-orbital (LMTO) method within the atomic-spheres approximation (ASA).[29] The valence wave functions are computed for the six valence bands at 505 **k** points within the first irreducible Brillouin zone. The core wave functions are solved also self-consistently, i.e., without the frozen-core approximation. Then, the momentum distribution for every Bloch state is calculated within the IPM using the LMTO-ASA method including the corrections to the overlapping spheres.[30] The valence and core contributions are multiplied by the state-dependent enhancement factors [Eq. (7)] calculated using the GGA partial annihilation rates [Eqs. (6) and (8)]. Finally all the contributions are summed up.

Figure 1(a) shows the Cu energy bands along the Γ-X direction in the first Brillouin zone and the corresponding behavior of the state-dependent enhancement. Only the bands that contribute to the momentum density within the first Brillouin zone are shown. The corresponding enhancement factors calculated within the GGA [Eq. (8)] are given in Fig. 1(b). Near the Γ point the enhancement for the d-type band (dashed line) is smaller than for the sp-type (solid line) band. When moving towards to the zone boundary, the hybridization of the bands increases the interstitial character of the d-type band and the corresponding enhancement factor increases. The opposite is true for the band which is sp-like near the Γ point. The results shown in Fig. 1(b) are in a qualitative agreement with those calculated by Sormann[16] with the exception that he does not obtain for the d-type band the strong decrease near the Γ point.

In Fig. 2 we show the (state-dependent) enhancements for all the calculated valence states of Cu as a function of en-

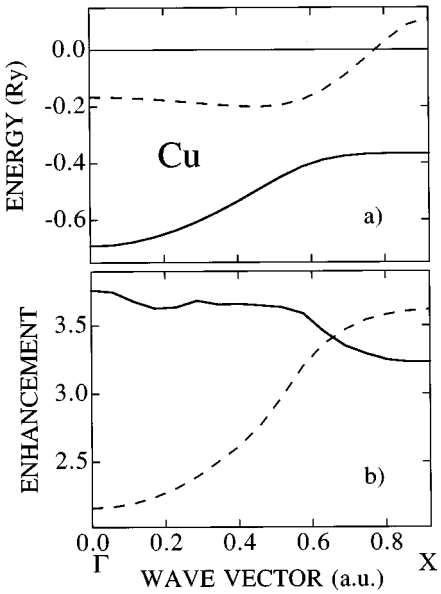

FIG. 1. (a) Electron band structure of Cu along the [100] direction in momentum space. Only the bands contributing to the momentum density of annihilating electron-positron pairs are shown. The energy zero coincides with the Fermi level. (b) State-dependent enhancement factor for the bands shown in (a). The solid (dashed) lines in (a) and (b) correspond to each other. Note that the enhancement factors for the states above the Fermi level are unphysical, because they are not occupied.

ergy. Because more states are shown than in Fig. 1 the minimum enhancement is slightly lower than that in Fig. 1. At low energies where the states have mainly *s* character the enhancement is large and fairly constant. In the intermediate energy region where the *d* character of the states is strong the enhancement factors show a clear, rapidly decreasing trend with increasing energy. This trend reflects the localization of the states closer to the nuclei when the character of the states changes from bonding to antibonding. Due to the hybridization the *s* character and the ensuing delocalization tendency of the states increase close to the Fermi energy. This is seen as the increase of the enhancement values. The horizontal lines in Fig. 2 correspond to the enhancement factors calcu-

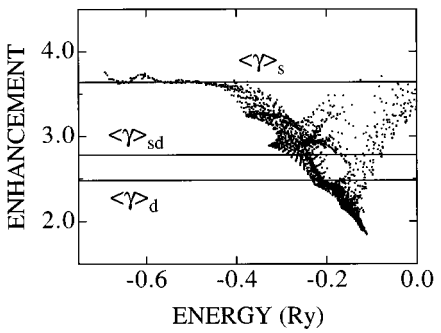

FIG. 2. Enhancement factors for the conduction band states in Cu. The horizontal lines give the values obtained using the atomic superposition method for the 4*s* ($\langle\gamma\rangle_s$) and 3*d* ($\langle\gamma\rangle_d$) electrons as well as their weighted average ($\langle\gamma\rangle_{sd}$). The energy zero coincides with the Fermi level.

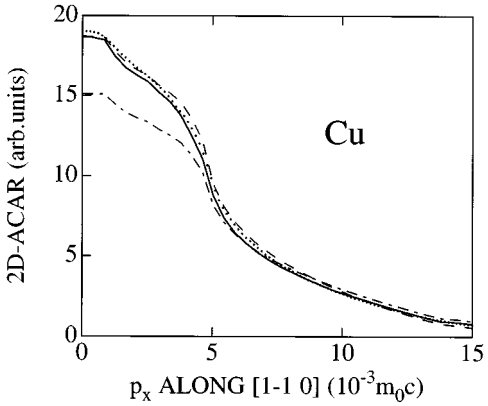

FIG. 3. 2D-ACAR spectra for Cu. The momentum densities are integrated in the [111] direction, and normalized to the same volume. Cuts along the [110] direction are given. The solid, dashed, and dash-dotted lines give the results in the present state-dependent enhancement scheme, in the GGA of Eq. (6), and in the IPM, respectively. The experimental points are shown by dots.

lated within the atomic superposition method.[31] In this method atomic electron densities (e.g., for 3*d* and 4*s* states) are used and therefore the enhancement factors are averages over the actual valence states. It can be seen that the enhancement factor for the atomic 4*s* state agrees well with the largest enhancement factors for the valence states, whereas the enhancement factor for the atomic 3*d* state seems to be close to the center of mass of the enhancement factors for all the valence states.

The 2D-ACAR maps $\rho(p_x,p_y)$ are obtained from the momentum distributions $\rho(\mathbf{p})$ by integrating in a given (z) direction,

$$\rho(p_x,p_y)=\int \rho(\mathbf{p})dp_z\,. \tag{9}$$

2D-ACAR maps calculated with different models are compared with the experimental map in Fig. 3. The LDA scheme of Eq. (5) gives qualitatively similar but in comparison with experiment slightly worse results than the GGA scheme of Eq. (6). Therefore the LDA results are not shown in Fig. 3. All the distributions are normalized to the same volume and integrated in the [111] direction of the fcc lattice. The core contributions are added in the theoretical results by using core wave functions which are self-consistent in the solid environment. The cuts of the two-dimensional maps along the [110] direction are given. The other directions give similar results. Comparing the curves obtained in the present state-dependent enhancement scheme and in the GGA scheme of Eq. (6) with the IPM result we see that the effect of the correlation is to localize the annihilation in the momentum space. In the GGA scheme of Eq. (6) this effect is due to the modification, $\psi_+(\mathbf{r})$ (IPM) $\rightarrow\psi_+(\mathbf{r})\sqrt{\gamma_{\mathrm{GGA}}(\mathbf{r})}$ (GGA), increasing the weight of the electron states residing mainly in the interstitial regions and having a low momenta. In the present scheme the weight $\sqrt{\gamma_i}$ for the electron-positron pair-wave function is larger when the interstitial character of the electron wave function is stronger. The GGA-position-dependent enhancement factor $\sqrt{\gamma_{\mathrm{GGA}}(\mathbf{r})}$ narrows the integrand in Eq. (1) (especially for the

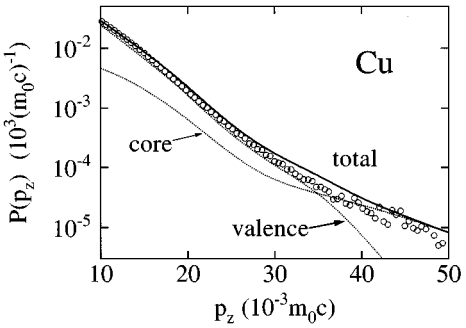

FIG. 4. Positron annihilation probability density $P(p_z)$ for Cu with p_z along the [111] direction. The experimental data (Ref. 6) (circles) and the theoretical result (solid line) obtained with the present state-dependent enhancement scheme are shown. The theoretical result is decomposed into the valence (sd) and to core contributions. The theoretical curves are convoluted with a Gaussian in order to mimic the finite experimental resolution.

valence states residing in the interstitial region). Therefore the momentum distributions obtained in this scheme are broader than those obtained in the new scheme.

One can see in Fig. 3 that the GGA result oscillates with respect to the experimental data. Moreover, the GGA scheme of Eq. (6) gives a distribution broader than the experimental one. This feature is hard to accept because the finite resolution ($\sim 0.8\times 10^{-3}m_0c$) has broadened the experimental distribution but is absent in the theoretical curves. The spurious oscillations are absent if the present scheme of the state-dependent enhancement is used. Moreover, the calculated distribution is shallower than the experimental one. Therefore the present scheme gives the best agreement with experiment.

Calculated one-dimensional momentum distributions can be compared with the Doppler spectra of the annihilating electron-positron pairs. In that case one has to integrate the momentum distribution $\rho(\mathbf{p})$ over two dimensions in order to obtain a one-dimensional dependence $\rho(p_z)$ and convolute it with a Gaussian with FWHM$=6.25\times 10^{-3}m_0c$ describing the experimental resolution. The theoretical momentum spectrum obtained in this way for Cu is compared with the experimental one[6] in Fig. 4. In this comparison p_z is along the [111] direction. The shapes of the theoretical and experimental distributions are in good agreement. Compared to the experiment, the calculation,[6] in which atomic $3d$ wave functions are used as core electron states, gives up to a factor of 2 too large a magnitude for the momentum distribution at momenta $\sim 15-40\times 10^{-3}m_0c$. The use of the solid d band states instead of the atomic states in these calculations does not change the distribution remarkably. Thus, it is important that the state dependence of the enhancement factor leads for the d-type states to a decreasing enhancement as a function of energy or the momentum of the state. However, the theoretical curve is at momenta $>\sim 18\times 10^{-3}m_0c$ slightly above the experimental points. This may indicate that the partial annihilation rates calculated with the GGA for the d-type bands are still too large.

B. Anisotropy of the momentum distribution

In order to study how well the present scheme describes the anisotropies in the momentum distributions at low momenta we have performed calculations for the III-V compound semiconductor GaAs. In this calculation the valence electron structure is obtained by using norm-conserving nonlocal pseudopotentials[32] and plane-wave expansions for the pseudovalence wave functions. The LMTO-ASA method would require in the case of GaAs the use of empty spheres centered around interstitial sites. The empty spheres cause difficulties in calculating the momentum distributions[33] and therefore we prefer to use the pseudopotential plane-wave method. The energy cutoff for the plane-wave expansions is 15 Ry. Electron states have been calculated for **k** points in a simple cubic mesh with a step of 0.147 a.u. $=1.07\times 10^{-3}m_0c$ in the [100] direction. The positron potential is constructed using the self-consistent pseudovalence electron density, the core electron densities of free atoms, and point like nuclear charges.[19] The positron wave function is solved in the real space.[34] The partial annihilation rates for the core states, including the Ga and As $3d$ bands, are calculated using the GGA [Eqs. (6) and (8)] and employing the LMTO-ASA method.[6] The partial annihilation rates for the valence states are calculated indirectly[35] within the GGA.

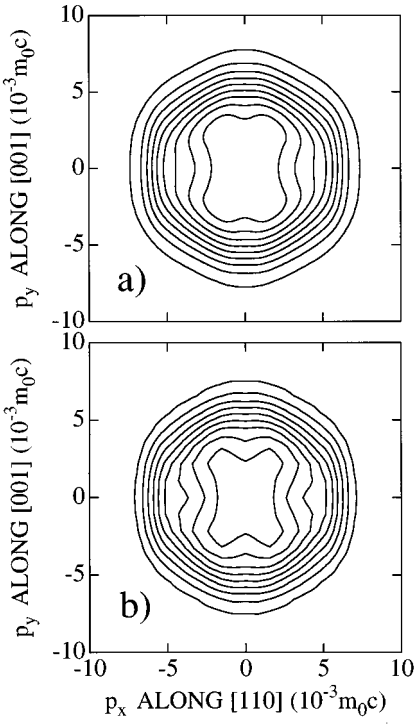

FIG. 5. Experimental (a) and theoretical (b) 2D-ACAR spectra for the perfect bulk GaAs lattice. The momentum distributions are integrated in the [110] direction and normalized to the same value at zero momentum. The contour spacing is one tenth of the maximum value.

The 2D-ACAR map calculated with the present state-dependent enhancement scheme is compared with the experimental one in Fig. 5. The momentum distributions are integrated in the [110] direction and normalized to the same value at the zero momentum. The normalization to the same volume cannot be used because the experimental 2D-ACAR data for GaAs is not accurate enough at momenta above $\sim 10\times 10^{-3}m_0c$. However, Fig. 5 shows that the agreement between theory and experiment is quite good at momenta below $\sim 10\times 10^{-3}m_0c$. The theoretical distribution is

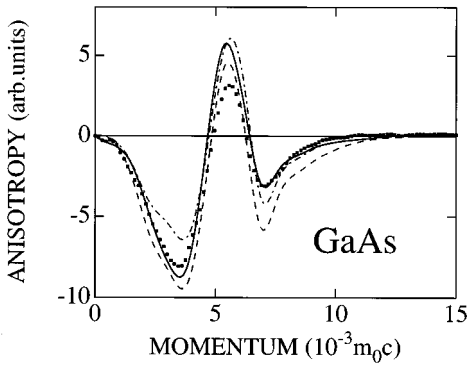

FIG. 6. Anisotropy of the 2D-ACAR spectra for the perfect bulk GaAs lattice. The momentum distributions are integrated in the [110] direction and normalized to the same value at zero momentum. The anisotropies are calculated as the differences between the distributions along the [110] and [001] directions. The solid, dashed, and dash-dotted lines are the results in the present state-dependent enhancement scheme, in the GGA of Eq. (6), and in the IPM, respectively. The experimental points are given by dots.

slightly narrower than the experimental one. In the [110] direction at momenta slightly less than $5\times10^{-3}m_0c$ the present scheme gives a plateau or a ''shoulder'' that is wider than that in the experimental data. The convolution of the theoretical curve with a Gaussian presenting the experimental resolution ($\sim0.8\times10^{-3}m_0c$) would smoothen the theoretical features.

Due to the above-discussed experimental difficulties at momenta above $\sim10\times10^{-3}m_0c$ we cannot compare magnitudes of the momentum distributions. However, in Fig. 6 we study the anisotropy of the momentum distribution by showing the differences between the cuts along the [110] and [001] directions. Relative to the IPM result, the inclusion of the correlation effects increases the magnitude of the anisotropy at small momenta, $2-5\times10^{-3}m_0c$, and improves the agreement with experiment. The ''shoulder'' seen in the [110] direction in Fig. 5 is reflected as a pronounced maximum in the anisotropy. At momenta above $6\times10^{-3}m_0c$ the present scheme reproduces quite faithfully the experimental points whereas the IPM and the GGA scheme of Eq. (6) give too large an anisotropy. For all momenta the curve corresponding to the GGA scheme of Eq. (6) is below those of the other theories. On the basis of Fig. 6, the use of the present state-dependent enhancement factor gives a clearly better agreement with experiment than the IPM or the GGA scheme of Eq. (6).

IV. CONCLUSIONS

We have introduced in the electron-positron momentum density calculations a parameter-free correlation scheme with state-dependent correction terms. The momentum distributions calculated agree rather well with the measured ones. This indicates that the form of the state dependence is adequate to account for most of the variations in the enhancement factor also as a function of the momentum of the annihilating electron-positron pairs. An explicit Kahana-type momentum-dependent enhancement factor is, according to these studies at least for Cu and GaAs, less important. For alkali metals this question remains still open. The present scheme is computationally tractable and can bring important results on electron-positron correlation effects in condensed matter. The knowledge of these effects is crucial for a proper interpretation of experimental spectra.

ACKNOWLEDGMENTS

The authors wish to thank P. Hautojärvi and K. Saarinen for discussions and S. Pöykkö for discussions and assistance in the plane-wave pseudopotential calculations. One of the authors (B.B.) was supported by the Swiss National Science Foundation Grant No. 8220-037167.

*Electronic address: bba@fyslab.hut.fi
†Electronic address: moh@fyslab.hut.fi
‡Electronic address: Martti.Puska@hut.fi
§Electronic address: Risto.Nieminen@hut.fi
‖Electronic address: Alfred.Manuel@physics.unige.ch

[1] S. Berko, in *Momentum Distributions*, edited by R. N. Silver and P. E. Sokol (Plenum, New York, 1989), p. 273.
[2] R. N. West, in *Positron Spectroscopy of Solids*, edited by A. Dupasquier and A. P. Mills, Jr. (IOS Press, Amsterdam, 1995), p. 75.
[3] M. Saito, A. Oshiyama, and S. Tanigawa, Phys. Rev. B **44**, 10 601 (1991).
[4] P. E. Mijnarends and A. Bansil, in *Positron Spectroscopy of Solids* (Ref. 2), p. 25.
[5] M. Šob, Mater. Sci. Forum **175–178**, 855 (1995).
[6] M. Alatalo, B. Barbiellini, M. Hakala, H. Kauppinen, T. Korhonen, M. J. Puska, K. Saarinen, P. Hautojärvi, and R. M. Nieminen, Phys. Rev. B **54**, 2397 (1996).
[7] S. Daniuk, G. Kontrym-Sznajd, J. Majers, A. Rubaszek, H. Stachowiak, P. A. Walters, and R. N. West, in *Positron Annihilation*, edited by P. C. Jain, R. M. Singru, and K. P. Gopinathan (World-Scientific, Singapore, 1985), pp. 43 and 279; J. Phys. F **17**, 1365 (1987); S. Daniuk, J. Phys.: Condens. Matter **1**, 5561 (1989).
[8] S. Berko, in *Positron Solid State Physics*, edited by W. Brandt and A. Dupasquier (North-Holland, Amsterdam, 1983), p. 64.
[9] J. P. Carbotte, in *Positron Solid State Physics* (Ref. 8), p. 32.
[10] J. Arponen and E. Pajanne, in *Positron Annihilation*, Proceedings ICPA7, edited by P. C. Jain *et al.* (World-Scientific, Singapore, 1985), p. 21.
[11] H. Stachowiak, Phys. Rev. B **41**, 12 522 (1990).
[12] B. Barbiellini, M. J. Puska, T. Torsti, and R. M. Nieminen, Phys. Rev. B **51**, 7341 (1995); B. Barbiellini, M. J. Puska, T. Korhonen, A. Harju, T. Torsti, and R. M. Nieminen, *ibid.* **53**, 16 201 (1996).
[13] S. Kahana, Phys. Rev. B **129**, 1622 (1963).
[14] E. Daniel and S. H. Vosko, Phys. Rev. **120**, 2041 (1960).
[15] L. Oberli, Ph.D. thesis, Geneva University, 1985; L. Oberli, A. A. Manuel, R. Sachot, P. Descouts, M. Peter, L. P. L. Rabou, P. E. Mijnarends, T. Hyodo, and A. T. Stewart, Phys. Rev. B **31**, 1147 (1985).
[16] H. Sormann, Phys. Rev. B **54**, 4558 (1996).

[17] T. Jarlborg and A. K. Singh, Phys. Rev. B **36**, 4660 (1987).
[18] L. Gilgien, G. Galli, F. Gygi, and R. Car, Phys. Rev. Lett. **72**, 3214 (1994).
[19] M. J. Puska, A. P. Seitsonen, and R. M. Nieminen, Phys. Rev. B **52**, 10 947 (1995).
[20] B. K. Panda, S. Fung, and C. D. Beling, Phys. Rev. B **53**, 1251 (1996).
[21] T. Jarlborg, B. Barbiellini, E. Boronski, P. Genoud, and M. Peter, J. Phys. Chem. Solids **52**, 1515 (1991).
[22] P. Pluvinage, J. Phys. Radium **12**, 799 (1951); O. Dulieu and C. le Sech, Europhys. Lett. **3**, 975 (1987).
[23] P. Asoka-Kumar, M. Alatalo, V. J. Ghosh, A. C. Kruseman, B. Nielsen, and K. G. Lynn, Phys. Rev. Lett. **77**, 2097 (1996).
[24] A. K. Singh, A. A. Manuel, T. Jarlborg, Y. Mathys, E. Walker, and M. Peter, Helv. Phys. Acta **59**, 410 (1986).
[25] A. A. Manuel, A. K. Singh, T. Jarlborg, P. Genoud, L. Hoffmann, and M. Peter, in *Positron Annihilation*, edited by L. Dorikens *et al.* (World-Scientific, Singapore, 1989), p. 833; P. Genoud, Ph.D. thesis, Geneva University, 1990.
[26] M. Šob, in *Proceedings of the Eighth Annual International Symposium on Electronic Structure of Metals and Alloys, Gaussig*, edited by P. Ziesche (Technische Universität, Dresden, 1978), p. 170; J. Phys. F **12**, 571 (1982); P. E. Mijnarends and R. M. Singru, Phys. Rev. B **19**, 6038 (1979).
[27] S. Wakoh, S. Berko, M. Haghgooie, and J. J. Mader, J. Phys. F **9**, L231 (1979).
[28] A. A. Manuel, S. Samoilov, Ø. Fischer, and M. Peter, Helv. Phys. Acta **52**, 255 (1979).
[29] O. K. Andersen, Phys. Rev. B **12**, 3060 (1975); G. Arbman and T. Jarlborg, J. Phys. F **7**, 1635 (1977).
[30] A. K. Singh and T. Jarlborg, J. Phys. F **15**, 727 (1985).
[31] M. J. Puska and R. M. Nieminen, J. Phys. F **13**, 333 (1983).
[32] G. B. Bachelet, D. R. Hamann, and M. Schlüter, Phys. Rev. B **26**, 4199 (1982); D. R. Haman, Bull. Am. Phys. Soc. **33**, 803 (1988). Our pseudopotentials are verified as ghost-free by the method by X. Gonze, R. Stumpf, and M. Scheffler, Phys. Rev. B **44**, 8503 (1991). We use the nonlinear core-valence exchange-correlation scheme by S. G. Louie, S. Froyen, and M. L. Cohen, *ibid.* **26**, 1738 (1982).
[33] B. Barbiellini and T. Jarlborg, Phys. Rev. B **50**, 3239 (1994).
[34] A. P. Seitsonen, M. J. Puska, and R. M. Nieminen, Phys. Rev. B **51**, 14 057 (1995).
[35] The partial annihilation rates for the valence states are first determined using the LDA for positron annihilation and then scaled to give with the GGA core annihilation rate the positron lifetime within the GGA. The GGA is not directly used to calculate the partial annihilation rates for valence electrons because a numerically stable determination of the gradient is difficult in a plane-wave basis. We have studied, by employing the LMTO-ASA method, the differences between the scaled LDA partial annihilation rates and those obtained directly within the GGA. The differences are small and can be omitted.